Low-frequency narrow-band acoustic filter with large orifice

Guancong Ma, Min Yang, Zhiyu Yang, and Ping Sheng

Citation: Applied Physics Letters **103**, 011903 (2013); doi: 10.1063/1.4812974
View online: http://dx.doi.org/10.1063/1.4812974
View Table of Contents: http://scitation.aip.org/content/aip/journal/apl/103/1?ver=pdfcov
Published by the AIP Publishing

Low-frequency narrow-band acoustic filter with large orifice

Guancong Ma,[1,a)] Min Yang,[1] Zhiyu Yang,[1,b)] and Ping Sheng[1,2]
[1]*Department of Physics, Hong Kong University of Science and Technology, Clear Water Bay, Kowloon, Hong Kong*
[2]*Institute of Advanced Study, Hong Kong University of Science and Technology, Clear Water Bay, Kowloon, Hong Kong*

(Received 15 April 2013; accepted 3 June 2013; published online 2 July 2013)

Conventional means of attenuating airborne sound usually require blocking the air medium with a solid material. By exploiting properties of membrane-type acoustic metamaterials (MAMs), we demonstrate large transmission loss to be achievable across a sizable orifice through which air can freely flow. We find that interaction of resonating field of the MAMs with the continuous sound field passing through the orifice is responsible for such phenomenon. The narrow-band characteristic of this effect can be used for acoustic filtering of noise with a particular narrow frequency band. © *2013 AIP Publishing LLC*. [http://dx.doi.org/10.1063/1.4812974]

Acoustic metamaterials are artificially engineered sub-wavelength structures that can affect the propagation of acoustic wave in ways not found in Nature. Over the past decade, exciting researches on acoustic metamaterials, such as super collimation,[1,2] acoustic focusing,[3,4] magnification and imaging beyond diffraction limit,[5–7] acoustic cloaking,[8–10] super absorption,[11] one-way transmission,[12,13] have been experimentally demonstrated. Exotic effective constitutive parameters[14–22] are almost always at the core of these studies.

It is usually the case that a hole with a sizable cross-sectional area in an otherwise impermeable solid wall would significantly reduce its sound transmission loss (STL, defined as $\mathrm{STL} = -20\log\frac{|P_t|}{|P_i|}$, where P_t and P_i are transmitted and incident pressure, respectively), even if the sound wavelength is much larger than the hole diameter. This is because the longitudinal nature of sound dictates that the wave passage through the hole (essentially a waveguide with a finite length) has no cutoff frequency, therefore at least one propagating mode can pass through. In this letter, we show by installing the surrounding area of the hole with membrane-type acoustic metamaterials (MAMs),[16] high STL can be achieved. We have identified the interaction between the resonant fields of the MAMs with the continuous field through the hole to be responsible for such abnormal transmission characteristics.

As shown in the left inset of Fig. 1, our device comprises four identical units of locally resonant MAMs[16] arranged around a circular orifice with radius R = 12 mm. Each MAM consists of a circular latex membrane, with radius R = 12 mm and 0.2 mm in thickness. The membrane is fixed around the edge, with a circularly symmetric pre-stress applied across its surface. A circular rigid disk with r = 4 mm, weighing 70 mg, is attached to the center of each membrane.

We use the modified impedance-tube method[23] to obtain the device's sound transmission characteristics. The apparatus consists of two Brüel & Kjær type-4206 impedance tubes, with the device firmly sandwiched in between. A loudspeaker is mounted at one end of the front tube. Two microphones are situated at two designated positions along the front tube. Two measurements at different locations in the front tube are necessary in order to separate the incident field from the reflected field. One microphone is positioned at the back tube to sense the transmitted field. To eliminate echoes, the back tube is terminated with ~25 cm thick anechoic sponge backed by an air-tight disk. The transmission coefficient of the device plotted as a function of frequency is shown in Fig. 1 (red solid curve). A sharp transmission dip is seen at 326 Hz, with $|t| = 0.037$ (29 dB in terms of STL). The dip is immediately followed by a small transmission peak, giving it an asymmetric shape. The dip has a very small bandwidth with STL vary by up to 24 dB within 15 Hz (from 326 Hz to 339 Hz). For reference, we used aluminum plates to block all four MAMs and obtained the transmission spectrum of the orifice itself. The STL difference between the two cases is 23 dB at 326 Hz.

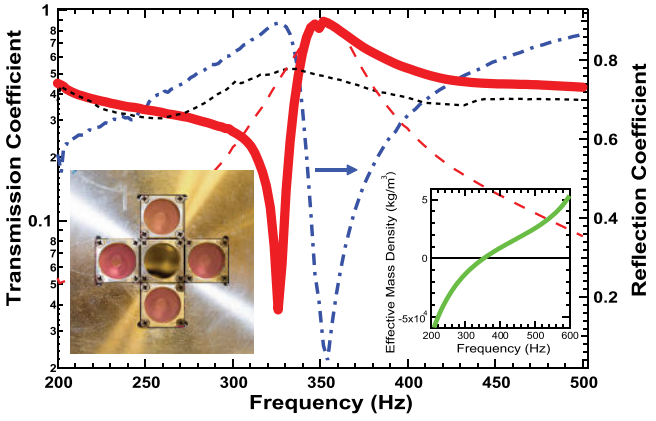

FIG. 1. Transmission and reflection spectra of the acoustic filter. Red solid curve is the experimental amplitude transmission coefficient (left axis). Blue dotted-dashed curve is the reflection coefficient (right axis). The transmission coefficient of the four MAMs' (with the central hole closed) is represented with red dashed curve (left axis). The amplitude transmission coefficient of the orifice alone is also plotted as a reference (black broken curve, left axis). The left inset is a photo image of the device. The inset on the right shows the calculated effective mass density (green solid curve).

[a)]Electronic mail: phmgc@ust.hk
[b)]Electronic mail: phyang@ust.hk

It is apparent that the sharp dip is due to the special feature of the MAMs around the orifice. We next closed the orifice, and measured the transmission spectrum of the four units of MAMs (Fig. 1). The transport property of the MAM is clearly dominated by a peak at 355 Hz, which is known to be the consequence of the 1st eigenmode resonance.[16,21,24] Trace of this resonant peak is also seen at the same frequency in the transmission spectrum of the entire device.

We are also able to experimentally map the out-of-plane displacement using a laser vibrometer (Graphtec AT500-05). We performed the experiment at two key frequencies: 326 Hz (transmission dip), and 355 Hz (transmission peak). It is seen that the MAM has a similar but off-phase vibrational profiles at these two frequencies. Such difference in the vibrational phase is intrinsic to the resonant nature of our MAM. The mechanical resonance is governed by a Lorentzian frequency response form, which mandates a phase change of π as the frequency sweeps across its eigenfrequency. This means that the system shifts from vibrating out-of-phase to in-phase with respect to the external harmonic excitation. Viewed from afar on the transmission side, the sub-wavelength-sized MAM is equivalent to a point source[21] which generates sound with 180° phase difference across its eigenfrequency. In contrast, the sound that passes through the orifice does not have such change in phase, since the small depth of the orifice dictates that its first Fabry-Perot-type mode must be located at a much higher frequency. Hence, low-frequency sound only accumulates a negligible phase in passing through the hole. As the MAMs and the central orifice are arranged closely together, the resonant field (by the metamaterials) and the continuous field (through the orifice) interfere and give rise to a Fano-like asymmetric dip-peak profile,[15,25,26] clearly observed in Fig. 1. At the transmission dip, the two fields destructively interfere, canceling the far-field transmission. This must be accompanied by a reflection maximum, also seen in Fig. 1.

The interference picture also explains the narrow band character of our device. The continuous field across the orifice has relatively high intensity. Only at frequencies very close to resonance can the off-phase field generated by the MAMs reach comparable intensity (see the dashed curves in Fig. 1) to completely counter the continuous field by destructive interference. On the other hand, once external stimulation passes the eigenfrequency, the MAMs' resonant field experiences a 180° phase change, and constructively interferes with the continuous field. Consequently, the dip must be very close to the peak, giving rise to a very narrow bandwidth.

We perform frequency-domain numerical simulations to confirm our analysis. The model was built using COMSOL MULTIPHYSICS, a commercial finite-element solver package. Since the device processes mirror symmetry, it is necessary to model only half of the device. In Fig. 2, we show cross-sectional slices of the calculated vibration profiles of the MAM as well as distribution of local velocity of air particles at the two key frequencies. A clear 180° phase difference in the MAM's displacement is seen, which is in agreement with experiment. Distinction in the local velocity (black arrow field) close to the metamaterial is also seen. At 326 Hz (Fig. 2(a)), namely, the dip's frequency, the phase of the field generated by the MAM is clearly opposite of the continuous field through the orifice. In this case, the air gains a horizontal velocity component and flows along the surface of the membrane, weakening the total energy that is radiated to the far field. However, the case is different for 355 Hz (Fig. 2(b)) at the transmission peak. The field by the MAM is in phase with respect to the field through the orifice, thereby enhancing the total transmitted wave.

The role of the MAMs can be further understood by using effective parameters. In this case, two constitutive parameters, effective mass density $\bar{\rho}$ and effective bulk modulus $\bar{\kappa}$, are relevant. Due to the extremely small thickness of our metamaterial, the excitation of monopolar motion (compression and expansion which will result in a change in volume) is impossible in the low-frequency regime, therefore $\bar{\kappa}$ should remain a constant, and does not deviate much from the static value of the bulk modulus of latex rubber (roughly 1.7×10^7 Pa[11]). The vibrational motion of the MAM's first eigenmode (Fig. 2)

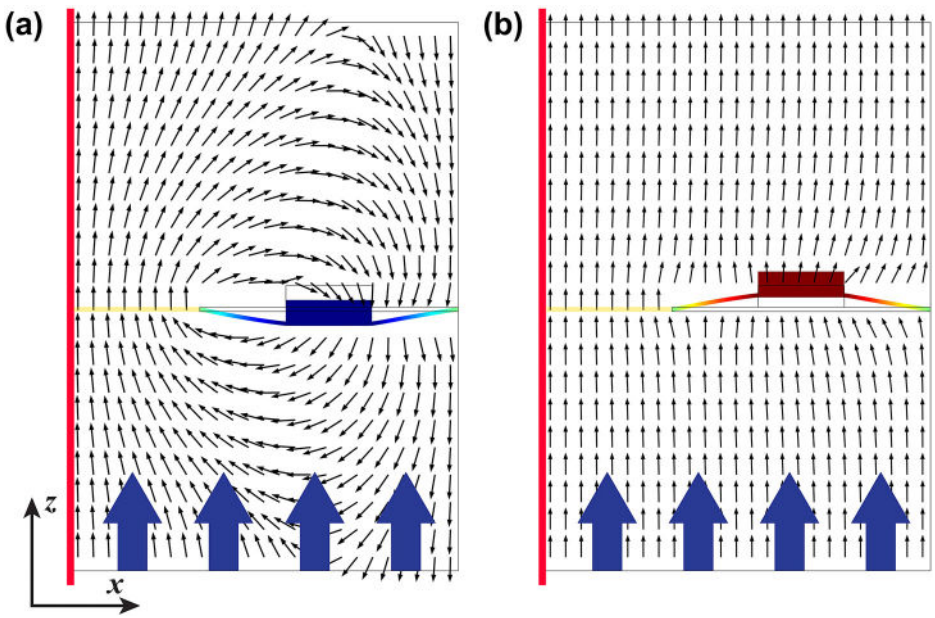

FIG. 2. Simulated field distribution and vibrational profiles at the 326 Hz transmission dip (a) and the 355 Hz transmission peak (b). The vertical straight red lines indicate the symmetry planes. The position of the orifice is indicated by the horizontal yellow lines. A plane wave is emitted from the bottom, represented by the large blue arrows. The black arrows show the direction of the air velocity. The length of the arrows is normalized for better viewing. The rainbow color represents the displacement along the z-direction of the metamaterial, with blue/green/red denoting negative/zero/positive displacements, respectively.

suggests a dominantly dipolar characteristic, hence we can expect an effective mass density that can differ significantly from its static value.[27] We have performed homogenization to extract $\bar{\rho}$, with the result shown by the green curve in the right inset in Fig. 1. (The detailed homogenization scheme can be found in the supplementary information of Ref. 22.) It is seen that $\bar{\rho}$ crosses zero at the eigenfrequency (355 Hz). Since $\bar{\kappa}$ remains a constant, the direct consequence of a vanishing $\bar{\rho}$ is that the effective impedance $|\bar{Z}| = |\sqrt{\bar{\rho}\bar{\kappa}}|$ is also vanishingly small. Therefore, the MAM's impedance matches well with the background air (which is very small) near the eigenfrequency, allowing the sound wave to be well coupled and transmitted. Moreover, a negative $\bar{\rho}$ region is found in the frequency regime before the 1st eigenfrequency. Negative-valued $\bar{\rho}$ indicates an imaginary effective wave vector $\bar{k} = i\omega\sqrt{|\bar{\rho}|/\bar{\kappa}}$, therefore sound wave is non-propagative in this regime. However, the decay length $d = i\bar{k}^{-1}$ can be large if $|\bar{\rho}|$ is small. At 326 Hz, we found that $d \approx 0.16$ m, which is much larger than the thickness of the MAM. Consequently, the evanescent wave is penetrative. Hence, we can expect a strong airborne propagative field in the air on the transmission side. In addition, negative-valued $\bar{\rho}$ means that the inertial response of the system would oppose the external excitation, thereby giving the transmitted field an extra phase of π with respect to the incident wave. It follows that at the edge of the 1st band gap, the field on the transmission side of the MAM can reach comparable amplitude with respect to the continuous field through the orifice. But the negative $\bar{\rho}$ also means that these two fields are out-of-phase with each other. Hence the two fields must destructively interfere, leading to peaked reflection and a sharp transmission dip, seen in Fig. 1.

Now, we understand the physics that is responsible for the transmission dip, we next demonstrate that a multi-frequency filter can also be realized. From the above discussion, we know that the transmission dip in our device shall be tunable by adjusting the eigenfrequency of the MAMs, which is adjustable by the weight of the central disks.[16,24] Based on the above-mentioned device, we further attach a 70 mg of mass (using sticky putty) to two units of the metamaterials, thereby shifting their eigenfrequency to ~248 Hz. The locally resonant nature of our metamaterials[16,21,22,24] ensures that the eigenmode of the remaining two units should be minimally affected. Measurements clearly show two sharp dips in the transmission spectrum: one at 242 Hz, while the other one remains at 340 Hz (Fig. 3). We note that the overall attenuation is slightly weakened ($|t| = 0.061$ at 1st dip, and $|t| = 0.056$ at 2nd dip) as compared with the previous single-frequency filter. This is because the reduction in the number of unit cells with a particular eigenfrequency inevitably decreases the total intensity of the off-phase sound field. The off-phase field may not reach the optimal intensity to give rise to a perfect destructive interference. However, this matter can be easily overcome by installing more MAMs around the orifice, or by increasing the cross-sectional area of the MAMs.

In summary, we have demonstrated a metamaterial-based acoustic device that can be used as a narrow-band acoustic filter for low-frequency applications. Compared with the traditional means of noise isolation, our acoustic filter has several advantages. First, it does not block air flow through the device. The sizable orifice can provide a wide range of utilities, including but not limited to air ventilation, heat exchange, weight reduction, or just for purely aesthetic purposes. Second, its effective frequency band width is extremely small. Moreover, it is possible to selectively filter multiple frequencies (but not in the sense of a broadband sound screen[11,24]) with one single layer of the device. These features make it ideal for isolation of noise with certain specific frequencies, such as noise in air ducts, noise from an engine/machinery, ambient noise in airliner's fuselage and ship's cabin. The narrow-band nature may also be exploited to add functionality, such as an alert mechanism for malfunctioning of machinery, since such events are usually accompanied by a change in the tone of noise.

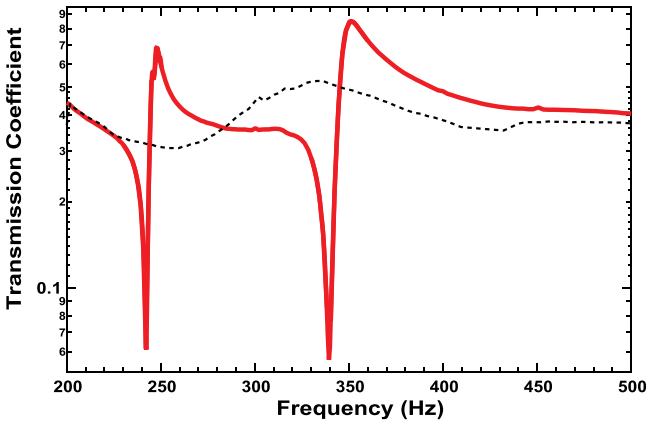

FIG. 3. Measured transmission coefficients of a dual-frequency acoustic filter device. Red solid curve is the amplitude transmission coefficient. The amplitude transmission coefficient of the orifice is also plotted as a reference (black broken curve).

The authors acknowledge the support of Hong Kong RGC Grant No. HKUST 604207, HKUST 606611, and HKUST2/CRF/11G.

[1]J. Christensen, A. I. Fernandez-Dominguez, F. de Leon-Perez, L. Martin-Moreno, and F. J. Garcia-Vidal, Nat. Phys. **3**, 851 (2007).
[2]J. Mei, B. Hou, M. Ke, S. Peng, H. Jia, Z. Liu, J. Shi, W. Wen, and P. Sheng, Appl. Lett. Phys. **92**, 124106 (2008).
[3]S. Zhang, L. Yin, and N. Fang, Phys. Rev. Lett. **102**, 194301 (2009).
[4]F. Lemoult, G. Lerosey, J. de Rosny, and M. Fink, Phys. Rev. Lett. **104**, 203901 (2010).
[5]J. Zhu, J. Christensen, J. Jung, L. Martin-Moreno, X. Yin, L. Fok, X. Zhang, and F. J. Garcia-Vidal, Nat. Phys. **7**, 52 (2011).
[6]J. Li, L. Fok, X. Yin, G. Bartal, and X. Zhang, Nature Mater. **8**, 931 (2009).
[7]F. Lemoult, M. Fink, and G. Lerosey, Phys. Rev. Lett. **107**, 064301 (2011).
[8]S. Zhang, C. Xia, and N. Fang, Phys. Rev. Lett. **106**, 024301 (2011).
[9]B. I. Popa, L. Zigoneanu, and S. A. Cummer, Phys. Rev. Lett. **106**, 253901 (2011).
[10]L. Sanchis, V. M. García-Chocano, R. Llopis-Pontiveros, A. Climente, J. Martínez-Pastor, F. Cervera, and J. Sánchez-Dehesa, Phys. Rev. Lett. **110**, 124301 (2013).
[11]J. Mei, G. Ma, M. Yang, Z. Yang, W. Wen, and P. Sheng, Nat. Commun. **3**, 756 (2012).
[12]B. Liang, X. S. Guo, J. Tu, D. Zhang, and J. C. Cheng, Nature Mater. **9**, 989 (2010).
[13]N. Boechler, G. Theocharis, and C. Daraio, Nature Mater. **10**, 665 (2011).
[14]Z. Liu, X. Zhang, Y. Mao, Y. Y. Zhu, Z. Yang, C. T. Chan, and P. Sheng, Science **289**, 1734 (2000).
[15]N. Fang, D. Xi, J. Xu, M. Ambati, W. Srituravanich, C. Sun, and X. Zhang, Nature Mater. **5**, 452 (2006).

[16]Z. Yang, J. Mei, M. Yang, N. H. Chan, and P. Sheng, Phys. Rev. Lett. **101**, 204301 (2008).
[17]Y. Lai, Y. Wu, P. Sheng, and Z. Q. Zhang, Nature Mater. **10**, 620 (2011).
[18]Y. Wu, Y. Lai, and Z. Q. Zhang, Phys. Rev. Lett. **107**, 105506 (2011).
[19]S. H. Lee, C. M. Park, Y. M. Seo, Z. G. Wang, and C. K. Kim, Phys. Rev. Lett. **104**, 054301 (2010).
[20]Y. M. Seo, J. J. Park, S. H. Lee, C. M. Park, C. K. Kim, and S. H. Lee, J. Appl. Phys. **111**, 023504 (2012).
[21]J. Mei, G. Ma, M. Yang, J. Yang, and P. Sheng. in *Acoustic Metamaterials and Phononic Crystals*, edited by Pierre A. Deymier (Springer, Berlin, Heidelberg, 2013), p. 159.
[22]M. Yang, G. Ma, Z. Yang, and P. Sheng, Phys. Rev. Lett. **110**, 134301 (2013).
[23]K. M. Ho, Z. Yang, X. X. Zhang, and P. Sheng, Appl. Acoust. **66**, 751 (2005).
[24]Z. Yang, H. Dai, N. Chan, G. Ma, and P. Sheng, Appl. Lett. Phys. **96**, 041906 (2010).
[25]C. Goffaux, J. Sánchez-Dehesa, A. L. Yeyati, P. Lambin, A. Khelif, J. O. Vasseur, and B. Djafari-Rouhani, Phys. Rev. Lett. **88**, 225502 (2002).
[26]F. Lemoult, N. Kaina, M. Fink, and G. Lerosey, Nat. Phys. **9**, 55 (2013).
[27]J. Li and C. T. Chan, Phys. Rev. E **70**, 055602(R) (2004).